NANO LETTERS

pubs.acs.org/NanoLett
Letter

Experimental Online Quantum Dots Charge Autotuning Using Neural Networks

Victor Yon,* Bastien Galaup, Claude Rohrbacher, Joffrey Rivard, Alexis Morel, Dominic Leclerc, Clément Godfrin, Ruoyu Li, Stefan Kubicek, Kristiaan De Greve, Eva Dupont Ferrier, Yann Beilliard, Roger G. Melko, and Dominique Drouin

Cite This: *Nano Lett.* 2025, 25, 3717−3725

Read Online

ACCESS | Metrics & More | Article Recommendations | Supporting Information

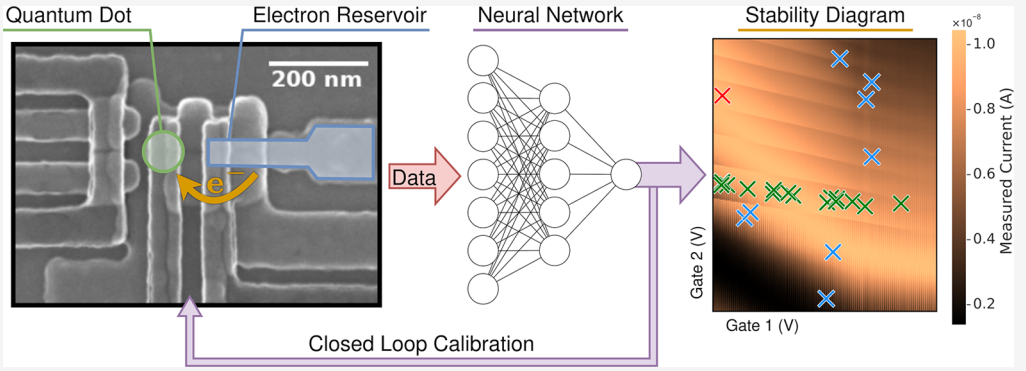

ABSTRACT: Spin-based semiconductor qubits hold promise for scalable quantum computing, yet they require reliable autonomous calibration procedures. This study presents an experimental demonstration of online single-dot charge autotuning using a convolutional neural network integrated into a closed-loop calibration system. The autotuning algorithm explores the gates' voltage space to localize charge transition lines, thereby isolating the one-electron regime without human intervention. This exploration leverages the model's uncertainty estimation to find the appropriate gate configuration with minimal measurements while reducing the risk of failures. In 20 experimental runs, our method achieved a success rate of 95% in locating the target electron regime, highlighting the robustness of this approach against noise and distribution shifts from the offline training set. Each tuning run lasted an average of 2 h and 9 min, primarily due to the limited speed of the current measurement. This work validates the feasibility of machine-learning-driven real-time charge autotuning for quantum dot devices, advancing the development toward the control of large qubit arrays.

KEYWORDS: *quantum dot, spin qubit, machine learning, convolutional neural network, scalable quantum computing, autonomous calibration, charge autotuning*

Semiconductor spin qubits[1−5] can encode quantum information using the spin-$\frac{1}{2}$ of a charge carrier, which can be manipulated using external magnetic fields to perform quantum computing based on the principles of superposition and entanglement. This technology stands out due to its high gate fidelity,[6−12] long coherence times,[13,14] thermal robustness,[15−17] and compatibility with existing complementary metal-oxide-semiconductor (CMOS) technologies.[18−22] These characteristics make spin qubits excellent candidates for building scalable quantum computers using already existing industrial fabrication methods.[22−25] However, significant engineering challenges remain, such as improving device fabrication quality[26−29] and developing autonomous calibration procedures for a large number of quantum dots (QDs).[30,31]

A spin qubit is formed by trapping a specific number of charge carriers within an isolated island (QD) using, for example, the electrostatic confinement gates of a nanoscale device (Figure 1a). Calibrating the QD device to achieve a specific physical state is a complex task that is generally approached in a series of sequential steps.[32] Initially, the device is cooled, local charge sensing systems are activated, and the voltages of the confinement gates are adjusted to operate within appropriate ranges for data collection.[33,34] Following

Received: October 2, 2024
Revised: February 11, 2025
Accepted: February 19, 2025
Published: February 27, 2025

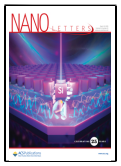

https://doi.org/10.1021/acs.nanolett.4c04889
Nano Lett. 2025, 25, 3717−3725

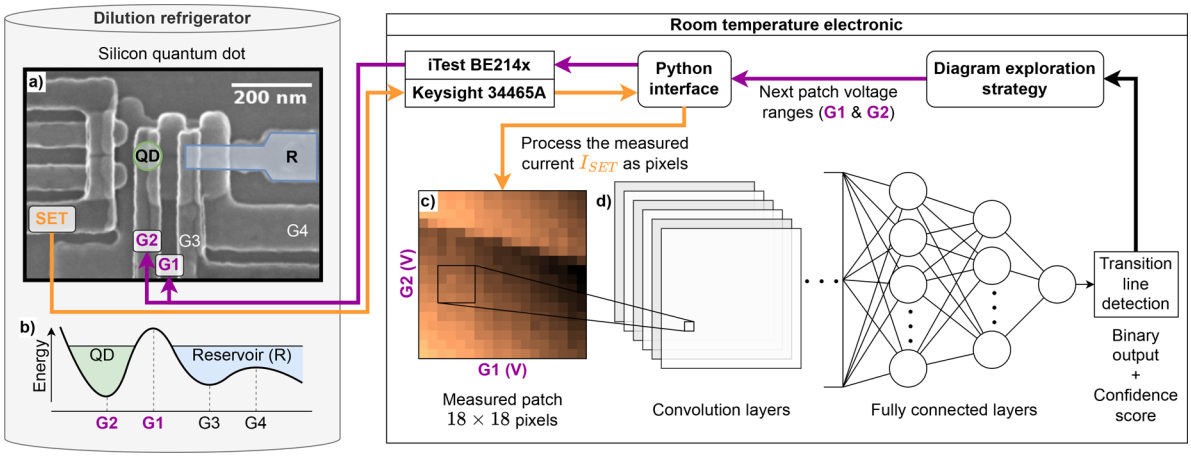

Figure 1. Schematic representation of the experimental setup. A silicon quantum dot (QD) device is cooled in a dilution refrigerator with a base temperature of 20 mk. The voltages at gates 3 (G3) and 4 (G4) are fixed, while a *iTest BE214x* controls the voltages at gates 1 (G1) and 2 (G2) through a Python interface. The scan coordinates are defined by an autonomous closed-loop procedure using a trained convolutional neural network (CNN) and an exploration strategy algorithm. **(a)** Scanning electron microscope (SEM) image of a silicon QD device with overlapping gates, similar to the one used during this experiment. The electrons flow from the reservoir (R) to the QD. See ref 66 for fabrication details. **(b)** Energy diagram representing the formation of a single QD in this device. **(c)** A subsection of the voltage space (referred to as "patch") was scanned by sweeping the voltages at gates G1 and G2 and measuring the current using the single-electron transistor (SET) connected to a *Keysight 34465A* multimeter. **(d)** Trained CNN that processed the measured patch through two convolutional layers and two fully connected layers to infer the presence of a transition line as a binary output.

this, the gate voltage ranges corresponding to a known global structure (such as single- or double-QD configurations) are calibrated. This step is usually referred to as coarse tuning.[35−42] Next, optional virtual gates could be established to compensate for capacitive crosstalk, ensuring precise control of the individual QDs without unwanted interference.[35,36,43−47] Subsequently, the device gate voltages are precisely tuned to achieve a specific charge carrier count in each QD, which in our experiment refers to the number of electrons in a single QD. This step is usually referred to as charge state tuning.[35,48−54] Finally, the system's physical parameters are refined in preparation for quantum computations.[36,55−57]

Performing an efficient and accurate calibration every time the system is cooled is critical to deploying large-scale QD-based systems. However, automatizing this process is challenging due to the sensitivity of the operational parameters, where each variable can affect others nonlinearly, exponentially increasing the complexity as the number of tuned devices grows. Variability in device fabrication adds another layer of difficulty, as each QD can behave differently, requiring customized tuning approaches. These devices and the measurement method are also susceptible to environmental conditions (e.g., thermal noise and electromagnetic interference), adding stochasticity to the measurements.

Recent progress in producing larger arrays of QDs[24,30] has accelerated the need for robust control procedures. This challenge has been partially addressed by leveraging machine learning (ML) models,[38,40] which can be used to tune quantum devices by automatically navigating through the large and noisy parameter space. However, ML methods, especially neural networks (NNs), are sensitive to the distribution shift[58] between the training and testing data and are well-known for unexpected failures.[59] Therefore, it is necessary to validate any NN-based autotuning method in a real-world experimental environment.[33] However, due to the scarcity and expense of the hardware required to run such experiments, most autotuning demonstrations are performed offline (i.e., using static prerecorded data). A few studies have demonstrated online experimental procedures for the first steps of the autotuning process: bootstrapping,[33] coarse tuning,[37,42] and creating virtual gates.[45,46] Baart et al.[53] showed an early demonstration of charge state autotuning using Gabor filters[60] and classical optimization algorithms, resulting in a single successful run after 3 h. Only Schuff et al.[61] ran and benchmarked online experiments that covered the full tuning procedure. Their method—based on a combination of tree search, Bayesian optimization, segmentation algorithms, and NNs—allowed them to reach 77% success over 13 runs for complete QD tuning. However, each run took an average of 38 h to complete due to the time required to measure large stability diagrams and the repeated calibration necessary after a stage failure.

The autotuning algorithm used during the experiment has been developed and tested offline in a previous study.[51] It relies on a convolutional neural network (CNN)[62−64] trained to detect charge transition lines in a small section of the stability diagram. The training is performed in a supervised manner on a data set[65] composed of static measurements made on similar silicon QD devices. Then, a closed-loop calibration procedure allows us to find the one-electron regime of a single QD by following an autonomous exploration strategy that leverages the CNN inference and uncertainty score. Exploiting the model's uncertainty improves the robustness of the autotuning by reducing the risk of critical failures caused by potential misclassifications[51] compared to classical ML methods.[32,48]

In this experiment, we successfully transfer the above ML-based charge autotuning method—developed using offline measurements—to real-time charge tuning on an experimental setup. The results confirm that the device-to-device variability and the resolution shift between the online and offline data do not negatively affect the line detection performance. We were also able to measure valuable information regarding the

https://doi.org/10.1021/acs.nanolett.4c04889
Nano Lett. 2025, 25, 3717−3725

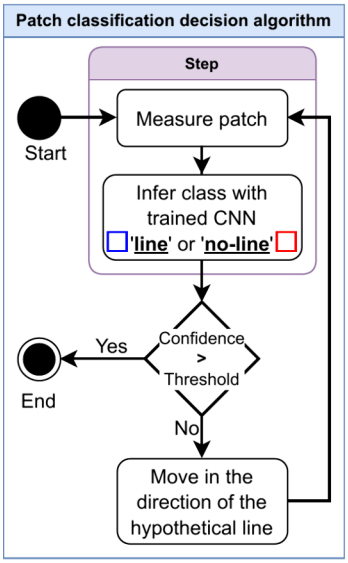

(a) Patch classification logic represented as a flow diagram.

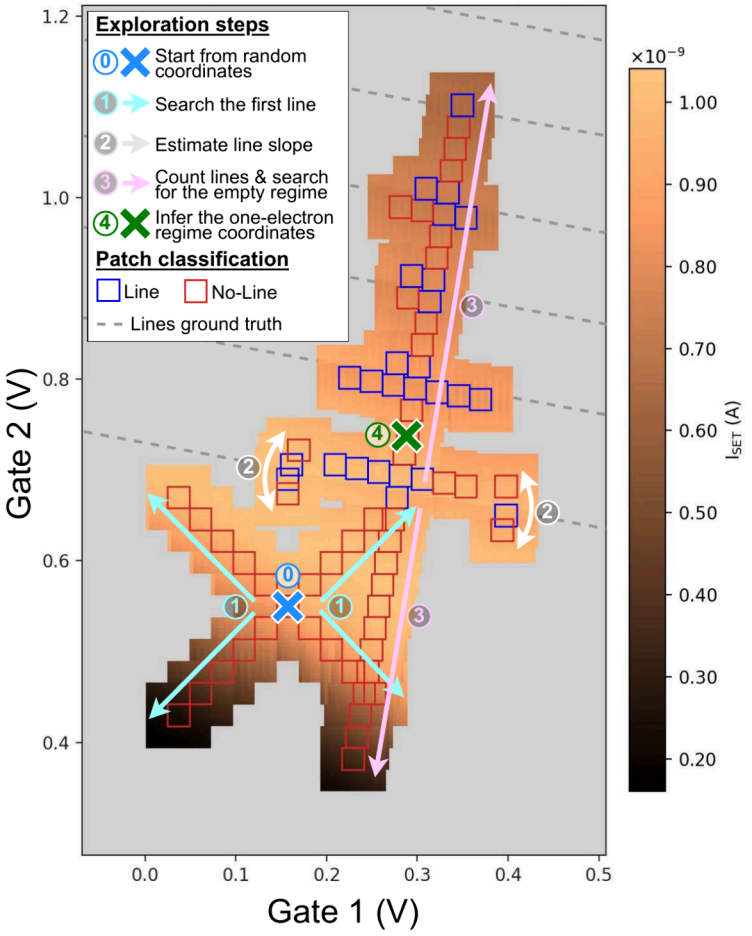

(b) Example of a successful online experimental autotuning.

Figure 2. Autonomous exploration strategy. One patch classification step of the algorithm is described in the subfigure (a). Multiple iterations of this step are represented by the blue and red squares in subfigure (b). In which, the arrows represent the direction of the exploration, and the gray area represents the unmeasured voltage space for this run. The cyan arrows *(1)* represent exploration in four directions to search for the first transition line. The white arrows in *(2)* represent the slope estimation step, performed by scanning two sections of the first detected line. Finally, the pink arrows *(3)* perpendicular to the estimated line slope represent the empty regime search *(down)* and the line count *(up)* procedure. A complete scan of this diagram is given in Figure 3a. See Supplementary Section S4 for more details regarding this autonomous exploration method.

autotuning duration and identify the current measurement as the time bottleneck.

The charge tuning process is typically guided by a stability diagram (two-dimensional current−voltage scan presented in Figure 3a), which is generated based on indirect QD measurements from a single-electron transistor (SET) for charge detection while sweeping the gate voltages. The transition lines (highlighted in green in Figure 3c) inform us of an electron movement between the reservoir and the QD (represented in Figure 1a,b). Given the knowledge that the QD is empty when no lines are visible at low gate voltages, it is possible to deduce the number of charges for a given position in the stability diagram (blue areas in Figure 3c). Although experts can perform manual tuning in small-scale experiments,[54] this is too slow and labor-intensive for large-scale industrial applications utilizing multiple QDs. Automating this task is necessary but challenging due to the noise induced by the environment and the measurement electronics, the device-to-device variability, and the variety of existing hardware implementations.

The autotuning is approached as an exploration problem, where we start from a random unknown position in the voltage space, gather information about the surroundings by performing local measurements, and search for the targeted charge regime. The transition lines guide the exploration by providing valuable information regarding the number of electrons in the QD. One exploration step consists of scanning a subsection of the voltage space (referred to as "patch" and represented in Figure 1c), sending it to the input of a CNN-based line detection model, and deciding the next area to explore based on an exploration strategy (see Figure 2). The patch size is fixed to 18 × 18 data points as a trade-off between the measurement time (a smaller area is faster to scan) and the line detection accuracy (a larger area simplifies the line detection). Due to the noisy nature of the measurements and the small size of the patch, classical signal processing and pattern detection methods[67−70] are not robust enough to reliably detect transition lines.[35,48,49,53] We opted for a supervised classification approach using a deep neural network (DNN),[71] which is known to be the best-performing method for pattern detection in noisy images.[62−64,72,73]

The line detection and exploration strategy are based on the autotuning method described in detail by Yon et al.[51] (see Supplementary Section S4). Nine stability diagrams, measured

https://doi.org/10.1021/acs.nanolett.4c04889
Nano Lett. 2025, 25, 3717−3725

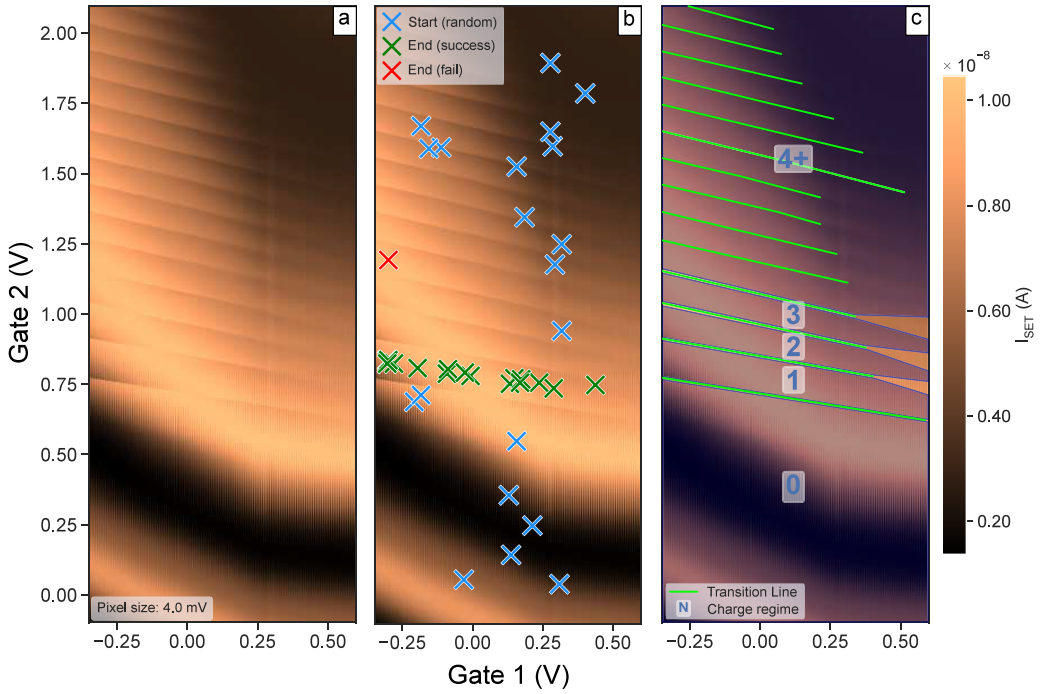

Figure 3. Complete scan of the explored stability diagram, processed after the experiment. (**a**) Representation of a stability diagram as an image, where pixel values encode the current measured using the single-electron transistor (SET) as a function of the gate voltages applied to the quantum dot (QD) (see Figure 1). (**b**) Start and end coordinates of the 20 online experimental autotuning runs. The blue crosses represent the random starting points of the runs. The green crosses represent the final coordinates of the successful autotuning runs (when the coordinates are inside the area annotated as a one-electron regime). The red cross represents the end coordinates of the run that did not reach the target regime. (**c**) Same diagram with manual annotations of transition lines in green and charge regime areas in blue. The region with four or more charges is annotated as "*4+*". The voltage areas not covered by a charge annotation (due to fading lines) are considered "*unknown charge regimes*".

during previous experiments on similar QD devices and manually annotated, are used to generate a training set of 33,429 patches. Each of these patches is categorized as "*line*" or "*no-line*" depending on whether an annotation of a transition line intersects with its center. More information on the diagram annotation and patch labeling is available in Supplementary Section S1. A CNN (represented in Figure 1d) is then optimized using gradient backpropagation[74] to classify patches in the training set (refer to Supplementary Section S2 for details on the training methodology).

The trained CNN is transferred to a computer connected to an *iTest BE214x* that is capable of controlling the voltage applied to each gate of the QD device and measuring the SET current by using a *Keysight 34465A* multimeter, as illustrated in Figure 1. The autotuning algorithm, implemented in Python,[1] plays a central role at each step of the exploration by *(i)* determining the next patch to measure based on the exploration strategy, *(ii)* transferring the voltage sweeping instructions to the multimeter, *(iii)* processing the measured current as a normalized image, and *(iv)* detecting a transition line by feeding the measured patch to the CNN input. To reduce the risk of tuning failures induced by potential patch misclassifications, each inference is associated with a confidence score that estimates the model's uncertainty for a given input. This score is calculated using a simple distance-based heuristic[75,76] (more information in Supplementary Section S3). When a patch is classified with a confidence score below the threshold, a verification procedure is automatically triggered to validate or refute the presence of a line in the surrounding area. This uncertainty-based exploration has been demonstrated to significantly improve the tuning success rate in offline experiments.[51] It is therefore expected to improve the robustness of autotuning in the case of unexpected perturbations related to the experimental context.

A silicon QD device with overlapping gates[66] was installed and cooled down in a dilution refrigerator with a base temperature of 20 mK. Once the device was cooled, we manually configured it in a single-QD state by keeping the voltages of the confinement gates and unused gates at 0 V, while applying 3 V to the gates we wanted to accumulate. These values were determined through standard I−V measurements. We then ran 20 consecutive and independent charge autotuning procedures.

Each run started at a random location (blue crosses in Figure 3b) in a voltage range of [−0.25 V, 0.5 V] for gate 1 (G1) (working range for the barrier gate between the QD and the reservoir, based on pinch-off measurement) and [0 V, 2 V] for gate 2 (G2) (working range for a single QD based on I−V charactrisations). Defining bounds on the gates' voltages was necessary to maintain the hardware's integrity and avoid wasting time on regions incompatible with a single-QD configuration. However, since the boundary values are generally consistent across all samples of the same type, characterization is required only on the first device.

The voltage space was then explored by using iterative patch measurements within the starting voltage ranges, extended by a 0.1 V margin in all directions to ensure the exploration did not begin near a boundary. We did not set virtual gates, as the tuning algorithm was designed to adapt to capacitive crosstalk. At the end of the experimental runs, we performed a complete scan of the explored area. The resulting stability diagram (shown in Figure 3a) was annotated by experts to identify the

https://doi.org/10.1021/acs.nanolett.4c04889
Nano Lett. 2025, 25, 3717−3725

transition lines and the charge areas (shown in Figure 3c). By placing the final coordinates of the 20 runs in this figure, we were able to count the number of times we reached the targeted one-electron regime.

Positioning the final voltage coordinates in a complete scan of the explored stability diagram (Figure 3a) allows us to evaluate which autotuning runs reach the targeted charge regime. Among the 20 experimental tunings performed, 19 (95%) successfully located the one-electron regime (green crosses in Figure 3b), while only 1 (5%) autotuning run failed (red cross in Figure 3b). An analysis of this failure revealed that it was caused not by patch misclassification but by a problem in the exploration logic related to the voltage boundaries. This issue has been fixed in the last version of the Python implementation. A visual animation of each run is available in a video.[2]

Each autotuning run took an average of 2 h and 9 min (standard deviation: 46 min) and 110 steps (standard deviation: 38) to complete. For comparison, scanning the full stability diagram presented in Figure 3a took approximately 7 h. Each step required 324 current measurements to obtain one patch (for 18 × 18 pixels), taking an average of 67 s using a *Keysight 34465A* multimeter, representing 96% of the process duration. Thus, data transfer and processing (including the CNN inference time) represent only a fraction of the tuning time. The high variability between run durations is attributable to the variable distance from the random starting point to the one-electron regime. The individual run statistics are available in Supplementary Table S3.

Prior offline benchmarks obtained by applying this autotuning method to similar devices led to a lower tuning success rate (78%)[51] despite the comparable line detection accuracy of the CNNs. The higher success rate obtained during this online experiment can be explained by several factors: *(i)* Online tuning allows us to precisely select the patch resolution, while offline diagrams need to be interpolated to compensate for the nonhomogeneous step size of the voltage sweeping between measurements (see comparison examples in Supplementary Section S6). This data processing is detrimental to measurement quality and could explain some line detection failures during offline tests. *(ii)* The fixed voltage range covered by offline diagrams often artificially increases the tuning difficulty by allowing for the exploration of irrelevant areas (e.g., beyond the barrier threshold). *(iii)* Offline autotuning experiments were performed on data measured from multiple devices, covering an extensive range of physical defects and measurement noise. The unique device used in this online experiment appears to be of good quality (e.g., low noise, no parasitic dots), providing optimal autotuning conditions.

This online experiment demonstrates the feasibility of autonomous real-time tuning based on ML. It validates that the expected distributional shift between the offline training data and the online measurements is not detrimental to the procedure's performance. On the contrary, the higher success rate observed in this experiment, compared to previous offline benchmarks on similar devices,[51] suggests that the absence of preprocessing improved the robustness of the autotuning. We also confirmed that the line detection model and the exploration strategy were versatile enough to successfully tune a QD device that was not in the training set.

The relatively slow tuning time (>2 h) does not satisfy the requirement for practical tuning of a large QD array. However, the SET measurement time, identified as the main bottleneck, could be drastically improved by optimizing the sensing method and hardware. For example, one could speed up the measurement time by a factor of 10 by implementing the measurement sequence on a dedicated processor[77] (e.g., a field-programmable gate array (FPGA)). This approach would cut the communication time between the instruments and the control computer, allowing for faster sweep rates. The radio frequency reflectometry technique[33,78] could also be used to speed up the charge sensing by measuring the impedance of the SET sensor at a fixed frequency, enabling single-shot readouts with only several microseconds of integration time.[79] This time can even be reduced to 400 ns with a Josephson parametric amplifier that also provides a high signal-to-noise ratio.[77] However, the whole measurement pipeline should be optimized to take advantage of this hardware acceleration, including data transfer, latency, and processing time. On the other hand, it is possible to limit the effect of this measurement bottleneck with a software approach; for example, by optimizing the meta-parameters (Supplementary Tables S1 and S2) in a way that reduces the number of measured points (e.g., smaller patches and a larger voltage distance between pixels) and reducing the number of steps (e.g., higher confidence threshold and smaller voltage boundaries). Finally, improving the fabrication processes of the QD chip is likely to reduce device-to-device variability, which will directly improve the autotuning robustness and reduce the number of steps by narrowing the voltage ranges to explore.

Further optimization can be achieved by moving the control electronics (represented in the right panel of Figure 1) to the cryogenic environment inside the dilution refrigerator. Bringing the control electronics closer to the tuned device, either by cointegrating them with the QD chip[22,25] or with additional nearby electronics, can reduce the parasitic capacitance added to the current measurements and allow for the control of large-scale arrays of QDs by circumventing the wiring bottleneck[80] between the QD devices and the control electronics. However, this *in situ* autotuning scheme requires the development of cryo-compatible and low-power custom electronics.[51,81−84]

■ ASSOCIATED CONTENT

Data Availability Statement

The Python source code used to aggregate and build the data set is publicly accessible on *GitHub*: https://github.com/3it-inpaqt/qdsd-dataset. The Python source code used to run all the experiments presented in this article is publicly accessible on *GitHub*: https://github.com/3it-inpaqt/dot-calibration-v2. The raw and processed stability diagram measurements used to train the line detection model for this experiment are publicly available for download from Yon et al.[65] The subset used to train the models in this paper is referred to as silicon overlapping gates quantum dot (Si-OG-QD). All trained models, experimental measurements, and results presented in this article are publicly available for download from Yon et al.[85]

Supporting Information

The Supporting Information is available free of charge at https://pubs.acs.org/doi/10.1021/acs.nanolett.4c04889.

Video of the 20 experimental runs (11 min) (MP4)

Data sets, the experiment methodology (model training, uncertainty and autonomous exploration strategy), individual run statistics and patches examples (PDF)

https://doi.org/10.1021/acs.nanolett.4c04889
Nano Lett. 2025, 25, 3717−3725

AUTHOR INFORMATION

Corresponding Author

Victor Yon − *Institut Interdisciplinaire d'Innovation Technologique (3IT) and Laboratoire Nanotechnologies Nanosystèmes (LN2) — CNRS 3463, Université de Sherbrooke, Sherbrooke, QC, Canada J1K 0A5; Institut quantique (IQ), Université de Sherbrooke, Sherbrooke, QC, Canada J1K 2R1;* orcid.org/0000-0003-4517-5042; Email: victor.yon@usherbrooke.ca

Authors

Bastien Galaup − *Institut Interdisciplinaire d'Innovation Technologique (3IT) and Laboratoire Nanotechnologies Nanosystèmes (LN2) — CNRS 3463, Université de Sherbrooke, Sherbrooke, QC, Canada J1K 0A5; Institut quantique (IQ), Université de Sherbrooke, Sherbrooke, QC, Canada J1K 2R1*

Claude Rohrbacher − *Laboratoire Nanotechnologies Nanosystèmes (LN2) — CNRS 3463, Université de Sherbrooke, Sherbrooke, QC, Canada J1K 0A5; Institut quantique (IQ) and Département de physique, Université de Sherbrooke, Sherbrooke, QC, Canada J1K 2R1;* orcid.org/0009-0003-5789-3807

Joffrey Rivard − *Laboratoire Nanotechnologies Nanosystèmes (LN2) — CNRS 3463, Université de Sherbrooke, Sherbrooke, QC, Canada J1K 0A5; Institut quantique (IQ) and Département de physique, Université de Sherbrooke, Sherbrooke, QC, Canada J1K 2R1*

Alexis Morel − *Laboratoire Nanotechnologies Nanosystèmes (LN2) — CNRS 3463, Université de Sherbrooke, Sherbrooke, QC, Canada J1K 0A5; Institut quantique (IQ) and Département de physique, Université de Sherbrooke, Sherbrooke, QC, Canada J1K 2R1*

Dominic Leclerc − *Laboratoire Nanotechnologies Nanosystèmes (LN2) — CNRS 3463, Université de Sherbrooke, Sherbrooke, QC, Canada J1K 0A5; Institut quantique (IQ) and Département de physique, Université de Sherbrooke, Sherbrooke, QC, Canada J1K 2R1*

Clément Godfrin − *IMEC, 3001 Leuven, Belgium*

Ruoyu Li − *IMEC, 3001 Leuven, Belgium*

Stefan Kubicek − *IMEC, 3001 Leuven, Belgium*

Kristiaan De Greve − *IMEC, 3001 Leuven, Belgium*

Eva Dupont Ferrier − *Laboratoire Nanotechnologies Nanosystèmes (LN2) — CNRS 3463, Université de Sherbrooke, Sherbrooke, QC, Canada J1K 0A5; Institut quantique (IQ) and Département de physique, Université de Sherbrooke, Sherbrooke, QC, Canada J1K 2R1*

Yann Beilliard − *Institut Interdisciplinaire d'Innovation Technologique (3IT) and Laboratoire Nanotechnologies Nanosystèmes (LN2) — CNRS 3463, Université de Sherbrooke, Sherbrooke, QC, Canada J1K 0A5; Institut quantique (IQ), Université de Sherbrooke, Sherbrooke, QC, Canada J1K 2R1*

Roger G. Melko − *Department of Physics and Astronomy, University of Waterloo, Waterloo, ON, Canada N2L 3G1; Perimeter Institute for Theoretical Physics, Waterloo, ON, Canada N2L 2Y5*

Dominique Drouin − *Institut Interdisciplinaire d'Innovation Technologique (3IT) and Laboratoire Nanotechnologies Nanosystèmes (LN2) — CNRS 3463, Université de Sherbrooke, Sherbrooke, QC, Canada J1K 0A5; Institut quantique (IQ), Université de Sherbrooke, Sherbrooke, QC, Canada J1K 2R1*

Complete contact information is available at: https://pubs.acs.org/10.1021/acs.nanolett.4c04889

Author Contributions

All authors contributed to this article and approved of the submitted version. Victor Yon: methodology, software implementation, experiments, results analysis and visualization, writing−original draft preparation. Bastien Galaup: software implementation, experiments, manuscript review. Claude Rohrbacher, Joffrey Rivard, Alexis Morel, and Dominic Leclerc: initialize and configure the experimental setup, methodology, manuscript review. Clement Godfrin, Ruoyu Li, Stefan Kubicek, and Kristiaan De Greve: manufactured the devices, manuscript review. Roger Melko: supervision, manuscript review. Eva Dupont-Ferrier, Yann Beilliard, and Dominique Drouin: methodology, supervision, funding acquisition, manuscript review, editing.

Notes

The authors declare no competing financial interest.

ACKNOWLEDGMENTS

V.Y. acknowledges Christian Lupien's valuable technical assistance in interfacing the experimental hardware with Python. V.Y., B.G., Y.B., and D.D. acknowledge support from the National Science Engineering Research Council of Canada, Grant ALLRP 580722-22, and the Fonds de Recherche du Québec—Nature et Technologies, Grant 300253. C.R., J.R., A.M., D.L., and E.D.F. acknowledge support from the FRQNT établissement de la relève professorale, Grant 2020-NC-268397, and the CRSNG, Grant RGPIN-2020-0573. R.G.M. acknowledges support from NSERC and the Perimeter Institute for Theoretical Physics. Research at the Perimeter Institute is supported in part by the Government of Canada through the Department of Innovation, Science and Economic Development Canada and by the Province of Ontario through the Ministry of Economic Development, Job Creation and Trade.

ADDITIONAL NOTES

[1]Python source code: github.com/3it-inpaqt/dot-calibration-v2

[2]Online autotuning experiment video: youtu.be/zGIQWEZex0s

REFERENCES

(1) Loss, D.; DiVincenzo, D. P. Quantum computation with quantum dots. *Phys. Rev. A* **1998**, *57* (1), 120−126, DOI: 10.1103/physreva.57.120.

(2) Veldhorst, M.; Yang, C. H.; Hwang, J. C. C.; Huang, W.; Dehollain, J. P.; Muhonen, J. T.; Simmons, S.; Laucht, A.; Hudson, F. E.; Itoh, K. M.; Morello, A.; Dzurak, A. S. A two-qubit logic gate in silicon. *Nature* **2015**, *526* (7573), 410−414.

(3) Watson, T. F.; Philips, S. G. J.; Kawakami, E.; Ward, D. R.; Scarlino, P.; Veldhorst, M.; Savage, D. E.; Lagally, M. G.; Friesen, M.; Coppersmith, S. N.; Eriksson, M. A.; Vandersypen, L. M. K. A programmable two-qubit quantum processor in silicon. *Nature* **2018**, *555* (7698), 633−637.

(4) Burkard, G.; Ladd, T. D.; Pan, A.; Nichol, J. M.; Petta, J. R. Semiconductor spin qubits. *Rev. Mod. Phys.* **2023**, *95* (2), No. 025003, DOI: 10.1103/revmodphys.95.025003.

(5) Zwanenburg, F. A.; Dzurak, A. S.; Morello, A.; Simmons, M. Y.; Hollenberg, L. C. L.; Klimeck, G.; Rogge, S.; Coppersmith, S. N.; Eriksson, M. A. Silicon quantum electronics. *Rev. Mod. Phys.* **2013**, *85* (3), 961−1019.

(6) Takeda, K.; Kamioka, J.; Otsuka, T.; Yoneda, J.; Nakajima, T.; Delbecq, M. R.; Amaha, S.; Allison, G.; Kodera, T.; Oda, S.; Tarucha, S. A fault-tolerant addressable spin qubit in a natural silicon quantum dot. *Science Advances* **2016**, *2* (8), No. e1600694, DOI: 10.1126/sciadv.1600694.
(7) Yoneda, J.; Takeda, K.; Otsuka, T.; Nakajima, T.; Delbecq, M. R.; Allison, G.; Honda, T.; Kodera, T.; Oda, S.; Hoshi, Y.; Usami, N.; Itoh, K. M.; Tarucha, S. A quantum-dot spin qubit with coherence limited by charge noise and fidelity higher than 99.9%. *Nat. Nanotechnol.* **2017**, *13* (2), 102−106.
(8) Mills, A. R.; Guinn, C. R.; Gullans, M. J.; Sigillito, A. J.; Feldman, M. M.; Nielsen, E.; Petta, J. R. Two-qubit silicon quantum processor with operation fidelity exceeding 99%. *Science Advances* **2022**, *8* (14), No. eabn5130, DOI: 10.1126/sciadv.abn5130.
(9) Noiri, A.; Takeda, K.; Nakajima, T.; Kobayashi, T.; Sammak, A.; Scappucci, G.; Tarucha, S. A shuttling-based two-qubit logic gate for linking distant silicon quantum processors. *Nature Communications* **2022**, *13* (1), No. 5740, DOI: 10.1038/s41467-022-33453-z.
(10) Xue, X.; Russ, M.; Samkharadze, N.; Undseth, B.; Sammak, A.; Scappucci, G.; Vandersypen, L. M. K. Quantum logic with spin qubits crossing the surface code threshold. *Nature* **2022**, *601* (7893), 343−347.
(11) Weinstein, A. J.; Reed, M. D.; Jones, A. M.; Andrews, R. W.; Barnes, D.; Blumoff, J. Z.; Euliss, L. E.; Eng, K.; Fong, B. H.; Ha, S. D.; Hulbert, D. R.; Jackson, C. A. C.; Jura, M.; Keating, T. E.; Kerckhoff, J.; Kiselev, A. A.; Matten, J.; Sabbir, G.; Smith, A.; Wright, J.; Rakher, M. T.; Ladd, T. D.; Borselli, M. G. Universal logic with encoded spin qubits in silicon. *Nature* **2023**, *615* (7954), 817−822.
(12) Gilbert, W.; Tanttu, T.; Lim, W. H.; Feng, M.; Huang, J. Y.; Cifuentes, J. D.; Serrano, S.; Mai, P. Y.; Leon, R. C. C.; Escott, C. C.; Itoh, K. M.; Abrosimov, N. V.; Pohl, H.-J.; Thewalt, M. L. W.; Hudson, F. E.; Morello, A.; Laucht, A.; Yang, C. H.; Saraiva, A.; Dzurak, A. S. On-demand electrical control of spin qubits. *Nat. Nanotechnol.* **2023**, *18* (2), 131−136.
(13) Tyryshkin, A. M.; Tojo, S.; Morton, J. J. L.; Riemann, H.; Abrosimov, N. V.; Becker, P.; Pohl, H.-J.; Schenkel, T.; Thewalt, M. L. W.; Itoh, K. M.; Lyon, S. A. Electron spin coherence exceeding seconds in high-purity silicon. *Nat. Mater.* **2011**, *11* (2), 143−147.
(14) Veldhorst, M.; Hwang, J. C. C.; Yang, C. H.; Leenstra, A. W.; de Ronde, B.; Dehollain, J. P.; Muhonen, J. T.; Hudson, F. E.; Itoh, K. M.; Morello, A.; Dzurak, A. S. An addressable quantum dot qubit with fault-tolerant control-fidelity. *Nat. Nanotechnol.* **2014**, *9* (12), 981−985.
(15) Petit, L.; Russ, M.; Eenink, G. H. G. J.; Lawrie, W. I. L.; Clarke, J. S.; Vandersypen, L. M. K.; Veldhorst, M. Design and integration of single-qubit rotations and two-qubit gates in silicon above one kelvin. *Communications Materials* **2022**, *3* (1), No. 82, DOI: 10.1038/s43246-022-00304-9.
(16) Yang, C. H.; Leon, R. C. C.; Hwang, J. C. C.; Saraiva, A.; Tanttu, T.; Huang, W.; Camirand Lemyre, J.; Chan, K. W.; Tan, K. Y.; Hudson, F. E.; Itoh, K. M.; Morello, A.; Pioro-Ladrière, M.; Laucht, A.; Dzurak, A. S. Operation of a silicon quantum processor unit cell above one kelvin. *Nature* **2020**, *580* (7803), 350−354.
(17) Huang, J. Y.; Su, R. Y.; Lim, W. H.; Feng, M.; van Straaten, B.; Severin, B.; Gilbert, W.; Dumoulin Stuyck, N.; Tanttu, T.; Serrano, S.; Cifuentes, J. D.; Hansen, I.; Seedhouse, A. E.; Vahapoglu, E.; Leon, R. C. C.; Abrosimov, N. V.; Pohl, H.-J.; Thewalt, M. L. W.; Hudson, F. E.; Escott, C. C.; Ares, N.; Bartlett, S. D.; Morello, A.; Saraiva, A.; Laucht, A.; Dzurak, A. S.; Yang, C. H. High-fidelity spin qubit operation and algorithmic initialization above 1K. *Nature* **2024**, *627* (8005), 772−777.
(18) Maurand, R.; Jehl, X.; Kotekar-Patil, D.; Corna, A.; Bohuslavskyi, H.; Laviéville, R.; Hutin, L.; Barraud, S.; Vinet, M.; Sanquer, M.; De Franceschi, S. A CMOSs silicon spin qubit. *Nature Communications* **2016**, *7* (1), No. 13575, DOI: 10.1038/ncomms13575.
(19) Dumoulin Stuyck, N. I.; Li, R.; Godfrin, C.; Elsayed, A.; Kubicek, S.; Jussot, J.; Chan, B. T.; Mohiyaddin, F. A.; Shehata, M.; Simion, G.; Canvel, Y.; Goux, L.; Heyns, M.; Govoreanu, B.; Radu, I. P.. Uniform spin qubit devices with tunable coupling in an all-silicon 300 mm integrated process. In *2021 Symposium on VLSI Circuits*; IEEE, 2021 pp 1−2. DOI: 10.23919/vlsicircuits52068.2021.9492427.
(20) Zwerver, A. M. J.; Krähenmann, T.; Watson, T. F.; Lampert, L.; George, H. C.; Pillarisetty, R.; Bojarski, S. A.; Amin, P.; Amitonov, S. V.; Boter, J. M.; Caudillo, R.; Correas-Serrano, D.; Dehollain, J. P.; Droulers, G.; Henry, E. M.; Kotlyar, R.; Lodari, M.; Lüthi, F.; Michalak, D. J.; Mueller, B. K.; Neyens, S.; Roberts, J.; Samkharadze, N.; Zheng, G.; Zietz, O. K. Qubits made by advanced semiconductor manufacturing. *Nature Electronics* **2022**, *5* (3), 184−190, DOI: 10.1038/s41928-022-00727-9.
(21) Rochette, S.; Rudolph, M.; Roy, A.-M.; Curry, M. J.; Ten Eyck, G. A.; Manginell, R. P.; Wendt, J. R.; Pluym, T.; Carr, S. M.; Ward, D. R.; Lilly, M. P.; Carroll, M. S.; Pioro-Ladrière, M. Quantum dots with split enhancement gate tunnel barrier control. *Appl. Phys. Lett.* **2019**, *114* (8), No. 083101, DOI: 10.1063/1.5091111.
(22) Rohrbacher, C.; Rivard, J.; Ritzenthaler, R.; Bureau, B.; Lupien, C.; Mertens, H.; Horiguchi, N.; Dupont-Ferrier, E.. Dual operation of gate-all-around silicon nanowires at cryogenic temperatures: Fet and quantum dot. *arXiv*, 2023. DOI: 10.48550/arxiv.2312.00903.
(23) Gonzalez-Zalba, M. F.; de Franceschi, S.; Charbon, E.; Meunier, T.; Vinet, M.; Dzurak, A. S. Scaling silicon-based quantum computing using cmos technology. *Nature Electronics* **2021**, *4* (12), 872−884.
(24) Neyens, S.; Zietz, O. K.; Watson, T. F.; Luthi, F.; Nethwewala, A.; George, H. C.; Henry, E.; Islam, M.; Wagner, A. J.; Borjans, F.; Connors, E. J.; Corrigan, J.; Curry, M. J.; Keith, D.; Kotlyar, R.; Lampert, L. F.; Madzik, M. T.; Millard, K.; Mohiyaddin, F. A.; Pellerano, S.; Pillarisetty, R.; Ramsey, M.; Savytskyy, R.; Schaal, S.; Zheng, G. Probing single electrons across 300-mm spin qubit wafers. *Nature* **2024**, *629* (8010), 80−85.
(25) Rohrbacher, C.; Leclerc, D.; Rivard, J.; Ritzenthaler, R.; Lupien, C.; Mertens, H.; Horiguchi, N.; Dupont-Ferrier, E. Nanosheet transistors produced in 300 mm fabrication platform for quantum computing. 2024. To be published.
(26) Dodson, J. P.; Holman, N.; Thorgrimsson, B.; Neyens, S. F.; MacQuarrie, E. R.; McJunkin, T.; Foote, R. H.; Edge, L. F.; Coppersmith, S. N.; Eriksson, M. A. Fabrication process and failure analysis for robust quantum dots in silicon. *Nanotechnology* **2020**, *31* (50), 505001.
(27) Tahan, C. Opinion: Democratizing spin qubits. *Quantum* **2021**, *5*, 584.
(28) Michniewicz, J.; Kim, M. S. Leveraging off-the-shelf silicon chips for quantum computing. *Appl. Phys. Lett.* **2024**, *124* (26), No. 260502, DOI: 10.1063/5.0207162.
(29) Saraiva, A.; Lim, W. H.; Yang, C. H.; Escott, C. C.; Laucht, A.; Dzurak, A. S. Materials for silicon quantum dots and their impact on electron spin qubits. *Adv. Funct. Mater.* **2021**, *32* (3), No. 2105488, DOI: 10.1002/adfm.202105488.
(30) Borsoi, F.; Hendrickx, N. W.; John, V.; Meyer, M.; Motz, S.; van Riggelen, F.; Sammak, A.; de Snoo, S. L.; Scappucci, G.; Veldhorst, M. Shared control of a 16 semiconductor quantum dot crossbar array. *Nat. Nanotechnol.* **2023**, *19* (1), 21−27.
(31) Mouny, P.-A.; Dawant, R.; Dufour, P.; Valdenaire, M.; Ecoffey, S.; Pioro-Ladrière, M.; Beillard, Y.; Drouin, D. Towards scalable cryogenic quantum dot biasing using memristor-based dc sources. *arXiv*, 2024. DOI: 10.48550/arxiv.2404.10694.
(32) Zwolak, J. P.; Taylor, J. M. Colloquium: Advances in automation of quantum dot devices control. *Rev. Mod. Phys.* **2023**, *95* (1), No. 011006, DOI: 10.1103/revmodphys.95.011006.
(33) Zubchenko, A.; Middlebrooks, D.; Rasmussen, T.; Lausen, L.; Kuemmeth, F.; Chatterjee, A.; Zwolak, J. P. Autonomous bootstrapping of quantum dot devices. *arXiv*, 2024. DOI: 10.48550/arxiv.2407.20061.
(34) Kovach, T. J.; Schug, D.; Wolfe, M. A.; MacQuarrie, E. R.; Walsh, P. J.; Benson, J.; Friesen, M.; Eriksson, M. A.; Zwolak, J. P. Batis: Bootstrapping, autonomous testing, and initialization system for quantum dot devices. *arXiv* 2024. DOI: 10.48550/arXiv.2412.07676.

https://doi.org/10.1021/acs.nanolett.4c04889
Nano Lett. 2025, 25, 3717−3725

(35) Ziegler, J.; Luthi, F.; Ramsey, M.; Borjans, F.; Zheng, G.; Zwolak, J. P. Tuning arrays with rays: Physics-informed tuning of quantum dot charge states. *Physical Review Applied* **2023**, *20* (3), No. 034067, DOI: 10.1103/physrevapplied.20.034067.
(36) Liu, H.; Wang, B.; Wang, N.; Sun, Z.; Yin, H.; Li, H.; Cao, G.; Guoping, G. An automated approach for consecutive tuning of quantum dot arrays. *Appl. Phys. Lett.* **2022**, *121* (8), No. 084002, DOI: 10.1063/5.0111128.
(37) Zwolak, J. P.; McJunkin, T.; Kalantre, S. S.; Dodson, J. P.; MacQuarrie, E. R.; Savage, D. E.; Lagally, M. G.; Coppersmith, S. N.; Eriksson, M. A.; Taylor, J. M. Autotuning of double-dot devices in situ with machine learning. *Physical Review Applied* **2020**, *13* (3), No. 034075, DOI: 10.1103/physrevapplied.13.034075.
(38) Kalantre, S. S.; Zwolak, J. P.; Ragole, S.; Wu, X.; Zimmerman, N. M.; Stewart, M. D.; Taylor, J. M. Machine learning techniques for state recognition and auto-tuning in quantum dots. *npj Quantum Information* **2019**, *5* (1), No. 6, DOI: 10.1038/s41534-018-0118-7.
(39) Darulová, J.; Troyer, M.; Cassidy, M. C. Evaluation of synthetic and experimental training data in supervised machine learning applied to charge-state detection of quantum dots. *Machine Learning Science and Technology* **2021**, *2* (4), No. 045023.
(40) Moon, H.; Lennon, D. T.; Kirkpatrick, J.; van Esbroeck, N. M.; Camenzind, L. C.; Yu, L.; Vigneau, F.; Zumbühl, D. M.; Briggs, G. A. D.; Osborne, M. A.; Sejdinovic, D.; Laird, E. A.; Ares, N. Machine learning enables completely automatic tuning of a quantum device faster than human experts. *Nat. Commun.* **2020**, *11* (1), No. 4161, DOI: 10.1038/s41467-020-17835-9.
(41) Ziegler, J.; McJunkin, T.; Joseph, E. S.; Kalantre, S. S.; Harpt, B.; Savage, D. E.; Lagally, M. G.; Eriksson, M. A.; Taylor, J. M.; Zwolak, J. P. Toward robust autotuning of noisy quantum dot devices. *Physical Review Applied* **2022**, *17* (2), No. 024069, DOI: 10.1103/physrevapplied.17.024069.
(42) Severin, B.; Lennon, D. T.; Camenzind, L. C.; Vigneau, F.; Fedele, F.; Jirovec, D.; Ballabio, A.; Chrastina, D.; Isella, G.; de Kruijf, M.; Carballido, M. J.; Svab, S.; Kuhlmann, A. V.; Geyer, S.; Froning, F. N. M.; Moon, H.; Osborne, M. A.; Sejdinovic, D.; Katsaros, G.; Zumbühl, D. M.; Briggs, G. A. D.; Ares, N. Cross-architecture tuning of silicon and SiGe-based quantum devices using machine learning. *Sci. Rep.* **2024**, *14* (1), No. 17281, DOI: 10.1038/s41598-024-67787-z.
(43) Perron, J. K.; Stewart, M. D.; Zimmerman, N. M. A quantitative study of bias triangles presented in chemical potential space. *J. Phys.: Condens. Matter* **2015**, *27* (23), 235302.
(44) Hensgens, T. *Emulating Fermi-Hubbard physics with quantum dots*. PhD Thesis, Delft University of Technology, 2018. DOI: 10.4233/uuid:b71f3b0b-73a0-4996-896c-84ed43e72035.
(45) Hsiao, T.-K.; van Diepen, C. J.; Mukhopadhyay, U.; Reichl, C.; Wegscheider, W.; Vandersypen, L. M. K. Efficient orthogonal control of tunnel couplings in a quantum dot array. *Physical Review Applied* **2020**, *13* (5), No. 054018, DOI: 10.1103/physrevapplied.13.054018.
(46) van Diepen, C. J.; Eendebak, P. T.; Buijtendorp, B. T.; Mukhopadhyay, U.; Fujita, T.; Reichl, C.; Wegscheider, W.; Vandersypen, L. M. K. Automated tuning of inter-dot tunnel coupling in double quantum dots. *Appl. Phys. Lett.* **2018**, *113* (3), No. 033101, DOI: 10.1063/1.5031034.
(47) Rao, A. S.; Buterakos, D.; van Straaten, B.; John, V.; Yu, C. X.; Oosterhout, S. D.; Stehouwer, L.; Scappucci, G.; Veldhorst, M.; Borsoi, F.; Zwolak, J. P. Mavis: Modular autonomous virtualization system for two-dimensional semiconductor quantum dot arrays. *arXiv* 2024. DOI: 10.48550/arXiv.2411.12516.
(48) Czischek, S.; Yon, V.; Genest, M.-A.; Roux, M.-A.; Rochette, S.; Lemyre, J. C.; Moras, M.; Pioro-Ladrière, M.; Drouin, D.; Beilliard, Y.; Melko, R. G. Miniaturizing neural networks for charge state autotuning in quantum dots. *Machine Learning Science and Technology* **2021**, *3* (1), No. 015001.
(49) Lapointe-Major, M.; Germain, O.; Camirand Lemyre, J.; Lachance-Quirion, D.; Rochette, S.; Camirand Lemyre, F.; Pioro-Ladrière, M. Algorithm for automated tuning of a quantum dot into the single-electron regime. *Phys. Rev. B* **2020**, *102* (8), No. 085301, DOI: 10.1103/physrevb.102.085301.
(50) Durrer, R.; Kratochwil, B.; Koski, J.V.; Landig, A.J.; Reichl, C.; Wegscheider, W.; Ihn, T.; Greplova, E. Automated tuning of double quantum dots into specific charge states using neural networks. *Physical Review Applied* **2020**, *13* (5), No. 054019, DOI: 10.1103/physrevapplied.13.054019.
(51) Yon, V.; Galaup, B.; Rohrbacher, C.; Rivard, J.; Godfrin, C.; Li, R.; Kubicek, S.; De Greve, K.; Gaudreau, L.; Dupont-Ferrier, E.; Beilliard, Y.; Melko, R. G.; Drouin, D. Robust quantum dots charge autotuning using neural network uncertainty. *Machine Learning: Science and Technology* **2024**, *5* (4), No. 045034.
(52) Muto, Y.; Nakaso, T.; Shinozaki, M.; Aizawa, T.; Kitada, T.; Nakajima, T.; Delbecq, M. R.; Yoneda, J.; Takeda, K.; Noiri, A.; Ludwig, A.; Wieck, A. D.; Tarucha, S.; Kanemura, A.; Shiga, M.; Tomohiro, T. Visual explanations of machine learning model estimating charge states in quantum dots. *APL Machine Learning* **2024**, *2* (2), No. 026110, DOI: 10.1063/5.0193621.
(53) Baart, T. A.; Eendebak, P. T.; Reichl, C.; Wegscheider, W.; Vandersypen, M. K. Computer-automated tuning of semiconductor double quantum dots into the single-electron regime. *Applied Physics Lett.* **2016**, *108* (21), No. 213104, DOI: 10.1063/1.4952624.
(54) Meyer, M.; Déprez, C.; Meijer, I. N.; Unseld, F. K.; Karwal, S.; Sammak, A.; Scappucci, G.; Vandersypen, L. M. K.; Veldhorst, M. Single-electron occupation in quantum dot arrays at selectable plunger gate voltage. *Nano Lett.* **2023**, *23* (24), 11593−11600.
(55) Teske, J. D.; Humpohl, S. S.; Otten, R.; Bethke, P.; Cerfontaine, P.; Dedden, J.; Ludwig, A.; Wieck, A. D.; Hendrik, H. A machine learning approach for automated fine-tuning of semiconductor spin qubits. *Appl. Phys. Lett.* **2019**, *114* (13), No. 133102, DOI: 10.1063/1.5088412.
(56) Botzem, T.; Shulman, M. D.; Foletti, S.; Harvey, S. P.; Dial, O. E.; Bethke, P.; Cerfontaine, P.; McNeil, R. P. G.; Mahalu, D.; Umansky, V.; Ludwig, A.; Wieck, A.; Schuh, D.; Bougeard, D.; Yacoby, A.; Hendrik, H. Tuning methods for semiconductor spin qubits. *Physical Review Applied* **2018**, *10* (5), No. 054026, DOI: 10.1103/physrevapplied.10.054026.
(57) Daraeizadeh, S.; Premaratne, S. P.; Matsuura, A. Y.. Designing high-fidelity multi-qubit gates for semiconductor quantum dots through deep reinforcement learning. In *2020 IEEE International Conference on Quantum Computing and Engineering (QCE)*; IEEE, 2020; pp 30−36. DOI: 10.1109/qce49297.2020.00014.
(58) Gawlikowski, J.; Tassi, C. R. N.; Ali, M.; Lee, J.; Humt, M.; Feng, J.; Kruspe, A.; Triebel, R.; Jung, P.; Roscher, R.; Shahzad, M.; Yang, W.; Bamler, R.; Zhu, X. X. A survey of uncertainty in deep neural networks. *arXiv*, 2021. DOI: 10.48550/arxiv.2107.03342.
(59) Goodfellow, I. J.; Shlens, J.; Szegedy, C. Explaining and harnessing adversarial examples. *arXiv*, 2014. DOI: 10.48550/arxiv.1412.6572.
(60) Mehrotra, R.; Namuduri, K. R.; Ranganathan, N. Gabor filter-based edge detection. *Pattern Recognition* **1992**, *25* (12), 1479−1494.
(61) Schuff, J.; Carballido, M. J.; Kotzagiannidis, M.; Calvo, J. C.; Caselli, M.; Rawling, J.; Craig, D. L.; van Straaten, B.; Severin, B.; Fedele, F.; Svab, S.; Kwon, P. C.; Eggli, R. S.; Patlatiuk, T.; Korda, N.; Zumbühl, D.; Natalia, N. Fully autonomous tuning of a spin qubit. *arXiv*, 2024. DOI: 10.48550/arxiv.2402.03931.
(62) Krizhevsky, A.; Sutskever, I.; Hinton, G. E. Imagenet classification with deep convolutional neural networks. *Communications of the ACM* **2017**, *60* (6), 84−90.
(63) O'Shea, K.; Ryan, R. An introduction to convolutional neural networks. *arXiv*, 2015. DOI: 10.48550/arxiv.1511.08458.
(64) Patil, A.; Rane, M. *Convolutional Neural Networks: An Overview and Its Applications in Pattern Recognition*; Springer Singapore, 2020; pp 21−30. DOI: 10.1007/978-981-15-7078-0_3.
(65) Yon, V.; Galaup, B.; Roux, M.-A.; Genest, M.-A.; Rohrbacher, C.; Rivard, J.; Godfrin, C.; Li, R.; De Greve, K.; Rochette, S.; Camirand-Lemire, J.; Gaudreau, L.; Pioro-Ladrière, M.; Beilliard, Y.; Melko, R. G.; Dupont-Ferrier, E.; Dominique, D. Quantum dots

stability diagrams dataset. *Zenodo*, 2024. DOI: 10.5281/zenodo.11402792.
(66) Elsayed, A.; Shehata, M. M. K.; Godfrin, C.; Kubicek, S.; Massar, S.; Canvel, Y.; Jussot, J.; Simion, G.; Mongillo, M.; Wan, D.; Govoreanu, B.; Radu, I. P.; Li, R.; Van Dorpe, P.; De Greve, K. Low charge noise quantum dots with industrial cmos manufacturing. *npj Quantum Information* **2024**, *10* (1), No. 70, DOI: 10.1038/s41534-024-00864-3.
(67) Sun, R.; Lei, T.; Chen, Q.; Wang, Z.; Du, X.; Zhao, W.; Asoke, K. N. Survey of image edge detection. *Frontiers in Signal Processing*, *2*, **2022**. DOI: 10.3389/frsip.2022.826967.
(68) Mukhopadhyay, P.; Chaudhuri, B. B. A survey of hough transform. *Pattern Recognition* **2015**, *48* (3), 993−1010.
(69) Ding, L.; Goshtasby, A. On the canny edge detector. *Pattern Recognition* **2001**, *34* (3), 721−725.
(70) Bishop, C. M. *Pattern recognition and machine learning*, 1st ed.; Information Science and Statistics; Springer, 2006.
(71) LeCun, Y.; Bengio, Y.; Hinton, G. Deep learning. *Nature* **2015**, *521* (7553), 436−444.
(72) Voulodimos, A.; Doulamis, N.; Doulamis, A.; Protopapadakis, E. Deep learning for computer vision: A brief review. *Computational Intelligence and Neuroscience* **2018**, *2018*, No. 7068349.
(73) Cai, L.; Gao, J.; Zhao, D. A review of the application of deep learning in medical image classification and segmentation. *Annals of Translational Medicine* **2020**, *8* (11), No. ATM36944.
(74) Raúl, R. *The Backpropagation Algorithm*; Springer: Berlin, Germany, 1996; pp 149−182, DOI: 10.1007/978-3-642-61068-4_7.
(75) Zaragoza, H.; d'Alché Buc, F. Confidence measures for neural network classifiers. In *Proceedings of the Seventh International Conferenceon Information Processing and Management of Uncertainty in Knowlegde Based Systems*, July 1998, Paris, France.
(76) Mandelbaum, A.; Daphna, D. Distance-based confidence score for neural network classifiers. *arXiv*, 2017. DOI: 10.48550/arxiv.1709.09844.
(77) Stehlik, J.; Liu, Y.-Y.; Quintana, C.M.; Eichler, C.; Hartke, T.R.; Petta, J.R. Fast charge sensing of a cavity-coupled double quantum dot using a josephson parametric amplifier. *Physical Review Applied* **2015**, *4* (1), No. 014018, DOI: 10.1103/physrevapplied.4.014018.
(78) Liu, Y.-Y.; Philips, S. G. J.; Orona, L.A.; Samkharadze, N.; McJunkin, T.; MacQuarrie, E.R.; Eriksson, M.A.; Vandersypen, L. M. K.; Yacoby, A. Radio-frequency reflectometry in silicon-based quantum dots. *Physical Review Applied* **2021**, *16* (1), No. 014057, DOI: 10.1103/physrevapplied.16.014057.
(79) Reilly, D. J.; Marcus, C. M.; Hanson, M. P.; Gossard, A. C. Fast single-charge sensing with a rf quantum point contact. *Appl. Phys. Lett.* **2007**, *91* (16), No. 162101, DOI: 10.1063/1.2794995.
(80) Reilly, D. J. Challenges in scaling-up the control interface of a quantum computer. In *2019 IEEE International Electron Devices Meeting (IEDM)*; IEEE, 2019. DOI: 10.1109/iedm19573.2019.8993497.
(81) Mouny, P.-A.; Dawant, R.; Galaup, B.; Ecoffey, S.; Pioro-Ladrière, M.; Beilliard, Y.; Dominique, D. Analog programming of cmos-compatible Al_2O_3/TiO_{2-x} memristor at 4.2 K after metal-insulator transition suppression by cryogenic reforming. *Appl. Phys. Lett.* **2023**, *123* (16), No. 163505, DOI: 10.1063/5.0170058.
(82) Dawant, R.; Gaudreau, M.; Roy, M.-A.; Mouny, P.-A.; Valdenaire, M.; Gliech, P. Damascene versus subtractive line cmp process for resistive memory crossbars beol integration. *Micro and Nano Engineering* **2024**, *23*, No. 100251.
(83) Xue, X.; Patra, B.; van Dijk, J. P. G.; Samkharadze, N.; Subramanian, S.; Corna, A.; Wuetz, B. P.; Jeon, C.; Sheikh, F.; Juarez-Hernandez, E.; Esparza, B. P.; Rampurawala, H.; Carlton, B.; Ravikumar, S.; Nieva, C.; Kim, S.; Lee, H.-J.; Sammak, A.; Scappucci, G.; Veldhorst, M.; Sebastiano, F.; Babaie, M.; Pellerano, S.; Charbon, E.; Vandersypen, L. M. K. Cmos-based cryogenic control of silicon quantum circuits. *Nature* **2021**, *593* (7858), 205−210.
(84) Yon, V.; Marcotte, F.; Mouny, P.-A.; Dagnew, G. A.; Kulchytskyy, B.; Rochette, S.; Beilliard, Y.; Drouin, D.; Pooya, P. A cryogenic memristive neural decoder for fault-tolerant quantum error correction. *arXiv*, 2023 DOI: 10.48550/arxiv.2307.09463.
(85) Yon, V.; Galaup, B.; Melko, R. G.; Beilliard, Y., Drouin, D. Experimental online quantum dots charge autotuning using neural networks - output data, *Zenodo*, 2024. DOI: 10.5281/zenodo.13381665.

https://doi.org/10.1021/acs.nanolett.4c04889
Nano Lett. 2025, 25, 3717−3725